Speckle-Tracking Echocardiography in Cardio-Oncology and Beyond

Raymundo A. Quintana, MD
Linh P. Bui, MD
Rohit Moudgil, MD, PhD
Nicolas Palaskas, MD
Saamir Hassan, MD
Jun-ichi Abe, MD, PhD
Elie Mouhayar, MD
Syed Wamique Yusuf, MBBS
Antonieta Hernandez, MD
Jose Banchs, MD

Speckle-tracking echocardiography has enabled clinicians to detect changes in myocardial function with more sensitivity than that afforded by traditional diastolic and systolic functional measurements, including left ventricular ejection fraction. Speckle-tracking echocardiography enables evaluation of myocardial strain in terms of strain (percent change in length of a myocardial segment relative to its length at baseline) and strain rate (strain per unit of time). Both measurements have potential for use in diagnosing and monitoring the cardiovascular side effects of cancer therapy. Regional and global strain measurements can independently predict outcomes not only in patients who experience cardiovascular complications of cancer and cancer therapy, but also in patients with a variety of other clinical conditions. This review and case series examine the clinical applications and overall usefulness of speckle-tracking echocardiography in cardio-oncology and, more broadly, in clinical cardiology. **(Tex Heart Inst J 2020;47(2):96-107)**

From: *Department of Medicine (Drs. Bui and Quintana), University of Texas Medical School and Memorial Hermann Hospital; and Division of Medicine, Department of Cardiology (Drs. Abe, Banchs, Hassan, Hernandez, Moudgil, Mouhayar, Palaskas, and Yusuf), University of Texas MD Anderson Cancer Center; Houston, Texas 77030*

Dr. Quintana is now at Emory University School of Medicine, Atlanta, Georgia.

Address for reprints:
Jose Banchs, MD, Department of Cardiology, Unit 1451, UT MD Anderson Cancer Center, 1515 Holcombe Blvd., Houston, TX 77030

E-mail:
jbanchs@mdanderson.org

Noninvasive imaging plays a crucial role in the prevention, diagnosis, and treatment of cardiovascular disease in both cancer patients and cancer survivors. Among the different noninvasive imaging methods available, echocardiography is inexpensive, widely available, and radiation-free; moreover, during the last decade, temporal resolution has greatly improved. Therefore, it is considered the test of choice for evaluating heart disease and, now, mechanical function.

Cardiac mechanics integrate the diverse elastic and contractile forces of cardiac myocytes. Cardiac sarcomere structures have 3 different spatial orientations: longitudinal, radial, and circumferential. This arrangement enables efficient myocardial contraction, characterized by shortening, thickening, and twisting of the myocardium, which can be likened to wringing out a wet towel.[1] Whereas conventional echocardiography captures the thickening motion of radially oriented myocardial fibers, it cannot accurately show the shortening and twisting motions of longitudinally and circumferentially oriented fibers. Consequently, conventional echocardiography cannot fully differentiate between active and passive myocardial movement.[2]

Newer imaging methods such as speckle-tracking echocardiography (STE) and tissue-Doppler imaging (TDI) enable clinicians to detect changes in myocardial function, measured in terms of strain and strain rate, before they can detect changes in left ventricular ejection fraction (LVEF). Myocardial strain, or deformation, is the percent change in length of a myocardial segment relative to its length at baseline; strain rate is the rate of deformation (strain per unit of time).[2] Strain is represented by the following equation:

$$(L - L_0) / L_0,$$

where L is the instantaneous length and L_0 is the length corresponding to zero stress.[3] Negative strain represents shortening or compression; positive strain, lengthening or expansion.[4]

Both STE and TDI can provide global estimates of left ventricular (LV) mechanics as well as information about the 3 spatial dimensions of cardiac deformation.[5] Unlike TDI, however, STE exploits the multiple bright speckles that are produced by the reflection, refraction, and scattering of ultrasound beams and captured on a normal echocardiogram. Software for STE, regardless of vendor, can generate information on myocardial deformation by tracking these speckles frame-to-frame throughout the cardiac cycle. Speckle-tracking echocardiography is also angle-independent and thus less prone to intra- and interobserver variability.[6] Meta-analyses suggest that the

mean normal strain values derived by STE are –19.7% (95% CI, –18.9% to –20.4%) for global longitudinal strain (GLS), –23.3% (95% CI, –22.1% to –24.6%) for global circumferential strain (GCS), and 47.3% (95% CI, 43.6% to 51%) for global radial strain (GRS); note, however, that each STE software vendor will report its own suggested normal values.[7,8] A 2014 meta-analysis that included 5,721 patients with diverse cardiovascular diseases revealed that STE-derived GLS was better than LVEF at predicting all-cause mortality and major adverse cardiac events.[9]

During the last few decades, continued advances in cancer therapeutics have greatly improved the overall survival rate in cancer patients.[10] However, many agents have cardiotoxic side effects that can manifest themselves early or even years after treatment. These side effects depend not only on the chemotherapeutic drug and dosage used but also on the susceptibility of individual patients. Because a large number of cancer patients who experience a decrease in LVEF will not recover full cardiac function without early diagnosis and therapy, the use of STE has important clinical implications.[11-13] Speckle-tracking echocardiography can detect myocardial dysfunction before a decrease in LVEF and enables clinicians to predict which patients will eventually develop chemotherapy-related cardiac dysfunction (CRCD).[14,15]

Trastuzumab and anthracyclines are the 2 best-characterized drugs associated with CRCD. In patients with breast cancer who receive both, a >10% decrease in peak GLS and a decrease in radial strain measured by STE predict a symptom-associated decrease in LVEF within the next 3 to 6 months.[14,16,17] In a systematic review that included 1,504 cancer patients undergoing diverse chemotherapy regimens based on anthracyclines, trastuzumab, or both, STE was found to be prognostically superior to TDI.[18] The investigators for that review also demonstrated that a relative decline in GLS of 10% to 15% was a useful predictor of CRCD.[18] Another study in cancer patients who were treated with anthracycline-based regimens analyzed a torsional subepicardial LV deformation parameter denoted by LV twist.[13] The product of LV twist and GLS 6 weeks after chemotherapy was the best predictor of subsequent CRCD, followed by GLS alone.[13] Finally, in a small observational study that included 52 patients who had received trastuzumab, anthracyclines, or both and then experienced a ≥11% drop in GLS, β-blocker treatment was associated with a significant improvement (P <0.001) in STE-derived GLS and LVEF.[19] Only 14 patients in this group had a decrease in LVEF consistent with CRCD.[19] Consequently, myocardial deformation could help identify patients with early LV dysfunction.

This review will now focus on the clinical application of STE to various cardio-oncologic diseases and then present specific cases illustrating its use to detect and recognize typical patterns of GLS seen on STE-derived polar (or "bull's-eye") maps in cancer patients.

Cardio-Oncologic Diseases

Radiation-Induced Heart Disease

Radiation therapy (RT), either alone or in combination with other cancer therapies, has played a vital role in improving the survival of patients with thoracic malignancies such as breast cancer and Hodgkin lymphoma. However, exposing the cardiac field to radiation can injure cardiac structures, leading to coronary artery disease (CAD), cardiomyopathy, conduction abnormalities, valvulopathies, and pericardial disease.[20] Even a minimal dose of radiation increases the rate of heart disease. Each gray (Gy) increase in radiation is associated with a 7.4% increase in the incidence of ischemic heart disease, and this increased risk typically becomes apparent within the first 5 years after exposure and persists for at least 2 decades.[21]

The pathogenesis of radiation-induced heart disease involves diverse microvascular changes. Endothelial cells become more permeable, followed by neutrophil migration into the interstitial space, increased reactive oxygen species formation, DNA damage, inflammation, and eventually fibrosis.[22] The damage to affected coronary arteries is related to the maximal radiation dose distribution. Both the left anterior descending coronary artery (LAD) and right coronary artery (RCA) are primarily affected in patients receiving mantle field radiation. Radiation of left- and right-sided breast cancer tends to affect the mid-LAD and proximal RCA, respectively. Arterial stenosis caused by RT usually affects the coronary ostia.[23-26] Although not yet clinically tested for its diagnostic usefulness in patients with radiation-induced CAD, STE has proved diagnostically useful in patients with stable angina and normal LVEF. A decrease in regional longitudinal systolic strain can help identify the culprit coronary artery. In addition, GLS measured at rest enhances the diagnostic performance of exercise stress testing.[27]

Myocardial damage is another frequent complication of RT that can become apparent soon or several years after treatment. In one study of acute RT-induced cardiac dysfunction, women with left-sided breast cancer who received adjuvant RT experienced a decrease in GLS and strain rate that persisted for up to 6 weeks after completing treatment.[28] However, no changes in LVEF were observed during that time.[28] The changes in myocardial deformation appear to be dose-dependent. In another study, the largest decrease in regional strain was seen in the apical peak systolic strain and strain rate, measurements corresponding with the segment of the heart (in this case, the apex) subject to the highest radiation dose.[29] However, no concise dose-volume relationship for RT-induced cardiac dysfunction has yet

been determined.[30] In a study of long-term Hodgkin lymphoma survivors who received mediastinal RT with or without anthracyclines, STE was used to look at cardiac mechanics 2 decades after successful treatment. Global longitudinal strain was lower in patients who received RT plus anthracyclines (–16.1% ± 1.9%) or RT alone (–17.5% ± 1.7%) than in healthy control subjects (–20.4% ± 1.7%). Thus, RT combined with anthracyclines had an additional negative long-term effect on cardiac mechanics.[31] A more recent meta-analysis in cancer survivors confirmed that thoracic RT was associated with increased risk of heart failure at least 5 years after treatment.[32] The hazard ratios reported were 2.7 to 7.4 for Hodgkin lymphoma and 1.5 to 2.4 for breast cancer.[32] In prospective studies under way, investigators are using STE, among other noninvasive and invasive imaging methods, and a wide range of biomarkers to elucidate the effects and mechanisms of RT-induced heart disease.[33]

Infiltrative Cardiomyopathy

Infiltrative cardiomyopathies are rare, difficult to diagnose, associated with poor outcomes, and late-occurring in the clinical course of systemic illness. They are all characterized by the abnormal deposition of substances in the myocardial cells or the intercellular matrix of the myocardium, which, if left unchecked, can lead to heart failure and even restrictive cardiac physiology. Infiltrative cardiomyopathies frequently seen in oncologic patients are cardiac amyloidosis, iron-overload cardiomyopathy (IOC), and lymphomatous involvement of the myocardium. Speckle-tracking echocardiography has proved useful in the diagnosis and prognosis of infiltrative cardiomyopathies.

Cardiac amyloidosis is the infiltrative cardiomyopathy seen most often in cardio-oncology. A systemic disease usually diagnosed later in life,[34,35] amyloidosis is caused by the extracellular deposition of misfolded β-pleated fibrils, leading to tissue and organ damage.[36] The 2 most common types are transthyretin amyloidosis (ATTR) and immunoglobulin light-chain amyloidosis (AL). The transthyretin type often affects the elderly and in most cases involves only the heart.

Iron-overload cardiomyopathy occurs most often in cancer patients with bone marrow infiltration or hematologic malignancies who require recurrent blood transfusions, although it is classically associated with hemochromatosis.[37] Chronic systemic iron overload eventually leads to the deposition of iron in the myocardium and subsequent reactive oxygen species formation, mitochondrial damage, and cardiomyocyte death.[38] Lymphomatous myocardial involvement is seen at autopsy in 16% of patients with Hodgkin lymphoma and 18% of patients with non-Hodgkin lymphoma. Cardiac compromise occurs at a median of 20 months after initial lymphoma diagnosis.[39] Previous studies in patients with

IOC secondary to thalassemia major revealed a significant reduction in GCS, GRS, and global end-systolic rotation. These abnormalities in myocardial deformation were seen despite a normal T2 score >20 ms on cardiac magnetic resonance imaging scans, consistent with normal or minimal iron deposition.[40,41] These findings suggest that myocardial iron overload is not the only mechanism underlying IOC, although it does play a central role in its development.[42]

A worsening of longitudinal strain in IOC patients is the only independent predictor of adverse clinical events and death.[43] In both AL and ATTR, left ventricular GLS (LVGLS) is significantly reduced along the basal-to-apical gradient. Regional longitudinal strain is reduced mostly in the basal wall regions with apical sparing, leading to the typical "polar map" plot seen in color-coded LV strain displays.[44,45] Reduced GLS is an independent predictor of survival in AL, and a decline in apical longitudinal strain is an independent predictor of major cardiovascular events in both AL and ATTR.[46,47]

Valvular Heart Disease

The association between RT and valvular heart disease (VHD) has been well documented since the 1960s.[48] Multiple studies have shown an increased rate of VHD after thoracic RT.[24,49,50] Asymptomatic Hodgkin lymphoma survivors who received mediastinal RT were found to have VHD in 32% of cases at 6 years and 42% at 20 years.[51,52] As in the case of RT-induced CAD, the risk of VHD increases with higher radiation doses. In one study, for radiation doses of 30, 31–35, 36–40, and >40 Gy to a given valve, the approximate 30-year cumulative risk of VHD was 3%, 6.4%, 9.3%, and 12.4%, respectively.[53] Despite providing evidence that anthracyclines increased the risk of valvulopathy, most of the studies cited above did not reveal the type or severity of valvular dysfunction. Therefore, it was not possible to distinguish intrinsic valvular pathology from mitral regurgitation in the presence of anthracycline-induced cardiomyopathy.[54,55] This issue was addressed, however, by a cross-sectional study of lymphoma survivors who received high-dose anthracyclines with and without RT. In that study, the incidence of valvular disease (usually aortic valve degeneration) was greater in the chemotherapy-only group than in a healthy age- and sex-matched control group (14% vs 4%, *P*=0.002).[56]

Over the last few years, various studies have proved the usefulness of STE in predicting outcomes in patients with VHD and their need for early surgical referral. In asymptomatic patients with chronic severe primary mitral regurgitation, LVEF is the main determinant of surgical intervention. Current guidelines recommend surgery in this patient population when there is evidence of LV dysfunction, defined as an LVEF between 0.30 and 0.60 or an LV end-systolic diameter ≥40 mm

(class I, level of evidence B).[57,58] Despite early intervention, however, postoperative LV dysfunction still occurs. In one study, a GLS greater than –19.9% on STE was a major independent predictor of postoperative LV dysfunction in asymptomatic patients with chronic severe primary mitral regurgitation.[59] In another study, LVGLS was greater in patients who had severe mitral regurgitation but no significant LV dilation or dysfunction than it was in control subjects because of the left ventricle's hyperdynamic function during regurgitation.[60]

Left ventricular GLS measured by STE has also been shown to be important in the risk stratification of patients with moderate-to-severe primary mitral regurgitation and normal LVEF. In these patients, the absence of LV contractile reserve, defined as a >2% improvement in GLS during peak exercise, was associated with a 2-fold increase in risk of cardiac events.[61] In patients with asymptomatic severe aortic regurgitation, surgery is reasonable when the LVEF is ≥0.50 with severe LV dilation with an LV end-systolic dimension >5 cm or an indexed LV end-systolic diameter >2.5 cm/m² (class IIa, level of evidence B).[57,58] In a study of patients with chronic severe aortic regurgitation, preserved LVEF, and nondilated ventricles (LV end-systolic diameter index, <2.5 cm/m²), a decrease in LVGLS was significantly associated with increased long-term mortality (P <0.001), proving its prognostic value in this clinical situation.[62] In asymptomatic patients with chronic severe aortic stenosis and normal LVEF, GLS can independently predict mortality and the need for aortic valve replacement.[63,64] Although none of the VHD studies reviewed in this section included cancer patients or survivors, we think that the concepts described are also applicable to patients with cancer therapeutics–related VHD.

Pericardial Disease

Pericardial diseases are often seen in cardio-oncology practice. Involvement of the pericardium can manifest itself in a spectrum of syndromes, including pericarditis, pericardial effusion, tamponade, and constrictive pericarditis; and it usually has a major impact on overall outcomes. One study showed that pericarditis may be a marker of occult cancer and that it may predict increased risk of death after a cancer diagnosis.[65] Pericardial tumors, which are rarely primary, often result from metastatic lung and brain cancer, melanoma, and lymphoma. They are usually accompanied by recurrent pericardial effusions or tamponade and associated with a poor prognosis.

Both RT and diverse chemotherapeutic agents can cause pericardial disease.[66] Radiation-induced pericardial disease can manifest itself as pericarditis, pericardial effusion, delayed thickening, and constrictive pericarditis. Pericarditis can develop acutely after mediastinal irradiation at a dose >40 Gy.[67] Pericardial effusions are usually diagnosed months or years after mediastinal RT,

and these fibrinous exudates are often loculated.[22,68] Constrictive pericarditis presents as newly diagnosed congestive heart failure approximately 10 years after RT.[69]

Speckle-tracking echocardiography plays an important role in differentiating between constrictive pericarditis and restrictive cardiomyopathy. In patients with constrictive pericarditis, the circumferential strain, torsion, and early diastolic apical untwisting velocities are markedly reduced. In contrast, in patients with restrictive cardiomyopathy, the longitudinal strain is reduced.[70,71] In addition, detailed echocardiographic analysis of 3-layer longitudinal and circumferential strain and twist angle shows promise for helping to distinguish between various perimyocardial inflammatory syndromes, ranging from predominantly pericarditis to predominantly myocarditis.[72]

Case Reports

Various aspects of strain imaging provide information about cardiac mechanics and myocardial function. Ensuring that the myocardium is well traced on 2-dimensional images so that only myocardial—as opposed to pericardial—speckles are being tracked helps validate the strain data obtained in each particular study. Viewing the strain curves as a function of time and in comparison with the electrocardiogram (ECG) signal provides data about myocardial function throughout the cardiac cycle. However, evaluating all of these data in addition to interpreting the rest of a conventional echocardiogram takes considerable time, which may not be available in busy cardiology practices. A time-saving, beneficial alternative involves recognizing patterns of peak systolic strain on 17-segment polar maps, similar to interpreting the polar map of a myocardial perfusion study. In the medical literature and in clinical practice, longitudinal strain—as opposed to circumferential or radial strain—is the most frequently analyzed strain parameter.

In each of the following case reports, a distinctive polar map of GLS peak systolic strain derived by STE is presented, along with a narrative from the clinician's perspective. In each polar map, a dark red pattern indicates normal function; a lighter red or pink pattern, dysfunction; and a blue pattern, the worst dysfunction.

Patient 1

Normal Pattern. A 64-year-old man presented with shortness of breath that had persisted for several weeks and worsened over the previous 3 days. The patient's medical history included parotid gland stage IV carcinoma, dyslipidemia, and hypertension; 3 years previously, he had undergone percutaneous coronary intervention (PCI) with a drug-eluting stent to treat CAD in the distal LAD. Clinical and laboratory evalu-

ations revealed pneumonitis, pneumonia, and a mildly elevated troponin I level. Aspirin and ticagrelor that the patient had been taking were discontinued by his oncologist because of chronic thrombocytopenia. An echocardiogram showed an LVEF of 0.61 and a normal strain pattern (Fig. 1), supporting the clinician's suspicion of a noncoronary cause for the current abnormal troponin I biomarker findings. Over the next month, the patient's pulmonary issues responded appropriately to medical therapy, and he had no further cardiac issues.

The homogeneously red polar map (Fig. 1) indicated a normal longitudinal strain pattern in this patient. Used as a reference, this map highlights the glaring abnormalities in strain pattern seen on the polar maps in the following cases.

Patient 2

Three-Vessel Coronary Artery Disease. A 72-year-old man with ischemic cardiomyopathy, an LVEF of 0.30 to 0.35, and peripheral vascular disease presented with shortness of breath and coughing. The patient's medical history included transient ischemic attack, dyslipidemia, chronic obstructive pulmonary disease, carotid stenosis, squamous cell carcinoma and presumed primary lung tumor treated with chemotherapy and radiation (completed 2 years previously), and ongoing cardiologic monitoring for CAD. Cardiac catheterization 4 years before presentation had revealed a patent LAD,

50% stenosis in the RCA, and an occluded left circumflex coronary artery (LCx) with right-to-left collateral vessels. Cardiac positron emission tomograms at presentation showed an LVEF of 0.34 with inferior and inferolateral hypokinesis.

This patient's longitudinal strain polar map (Fig. 2) revealed a pattern of segmental dysfunction that matched the known coronary anatomy. The pink pattern indicated dysfunction in the RCA and LCx territories; the red band through the anteroseptal and apical wall segments indicated relative sparing of the LAD territory.
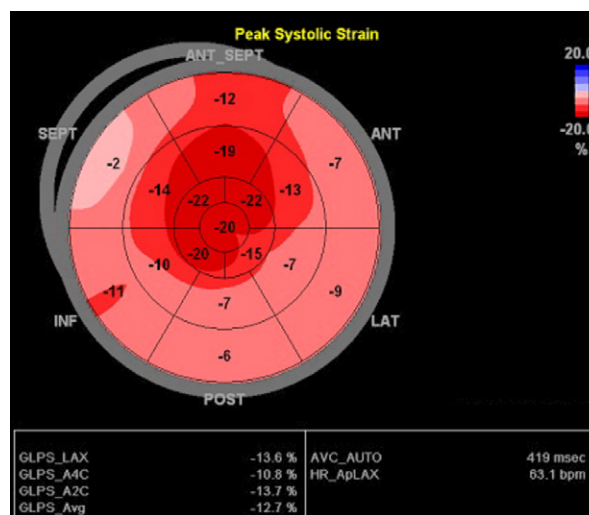
Patient 3

Single-Vessel Left Anterior Descending Coronary Artery Disease. A 48-year-old man with non-small cell lung cancer presented with chest pain. An ECG showed ST-segment elevations in the inferior leads and a QS pattern in the anterior leads. Cardiac enzyme levels were elevated. An echocardiogram showed hypokinesis of the inferior, anterior, and apical segments and an LVEF of 0.35 to 0.40. Emergency coronary angiograms revealed LAD occlusion with fresh thrombus, so PCI with bare-metal stenting was performed.

This patient's longitudinal strain polar map (Fig. 3) revealed defects in the LAD territory, as indicated by pink in the basal-to-mid segments and blue in the apical segments, whereas the rest of the polar map was homogeneously red. This pattern fits with a proximal-to-mid-
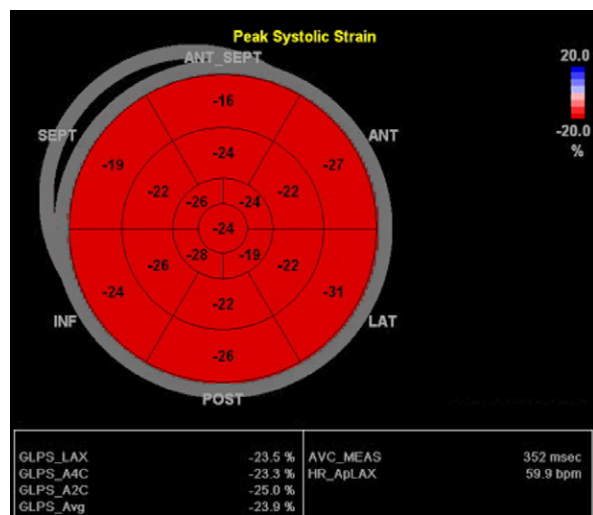
Fig. 1 *Patient 1. A polar map derived by speckle-tracking echocardiography shows a normal pattern of peak systolic strain of longitudinal myocardial fibers in a patient with a history of cancer and coronary artery disease. Note the homogeneous red pattern throughout, indicating normal function.*

ANT = anterior; ANT_SEPT = anteroseptal; ApLAX = apical long axis; AVC = aortic valve closure; Avg = average; A2C = apical 2-chamber view; A4C = apical 4-chamber view; bpm = beats per minute; GLPS = global longitudinal peak strain; HR = heart rate; INF = inferior; LAT = lateral; LAX = long axis; MEAS = measurement; POST = posterior; SEPT = septal

Fig. 2 *Patient 2. A polar map derived by speckle-tracking echocardiography shows the peak systolic strain of longitudinal myocardial fibers in a patient with 3-vessel coronary artery disease. The pattern of segmental dysfunction matches the patient's known coronary anatomy abnormalities.*

ANT = anterior; ANT_SEPT = anteroseptal; ApLAX = apical long axis; Avg = average; AVC = aortic valve closure; AUTO = automated measurement; A2C = apical 2-chamber view; A4C = apical 4-chamber view; bpm = beats per minute; GLPS = global longitudinal peak strain; HR = heart rate; INF = inferior; LAT = lateral; LAX = long axis; POST = posterior; SEPT = septal

LAD vessel occlusion causing substantial myocardial dysfunction distally in the vessel's territory, concordant with the angiographic findings in this case.

Patient 4

Single-Vessel Right Coronary Artery Disease. A 71-year-old man presented for prostatectomy. His medical history included basal cell carcinoma of the neck treated by resection 6 years previously and revision one year previously, prostate cancer, and CAD treated by remote angioplasty of the proximal RCA. The patient had been regularly evaluated by a local cardiologist, and his most recent nuclear stress test results showed no evidence of ischemia. The patient reported no symptoms of chest discomfort or palpitations. He had been relatively active, including walking 2 miles daily and using a push lawnmower without difficulty. An echocardiogram showed an LVEF of 0.45 to 0.50 and mild hypokinesis of the inferior wall.

This patient's polar map (Fig. 4), although slightly more subtle than a typical polar map in its depiction of the myocardial defect in pink rather than blue, showed a pink-to-light red pattern in the basal-to-mid segments of the RCA territory, as opposed to the deeper red pattern in other segments. This finding suggests residual myocardial dysfunction in the RCA territory after the

angioplasty, as corroborated by the inferior-wall hypokinesis seen echocardiographically. Of note, a nuclear stress test revealed normal perfusion and function, apparently missing the myocardial dysfunction seen on echocardiograms.
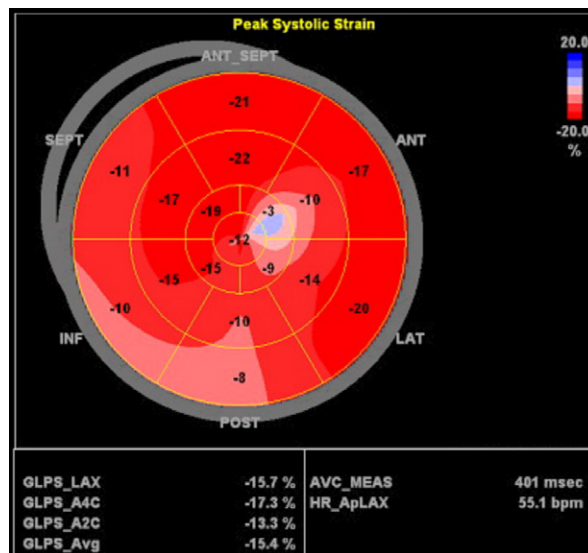
Patient 5

Single-Vessel Left Circumflex Coronary Artery Disease. A 67-year-old man with a history of metastatic prostate cancer and skin cancer was admitted for resection of a recurrent leiomyosarcoma of the right parietal and frontal scalp. Postoperatively, the patient had an episode of hypotension marked by systolic blood pressure reaching a nadir of 70 mmHg, ECG changes (ST-segment depression in the anterior and lateral leads), and elevated cardiac enzyme levels. The patient reported no chest pain, dizziness, or shortness of breath, and he had no history of cardiac disease. An echocardiogram showed an LVEF of 0.45 to 0.50 and mild hypokinesis of the lateral wall. Coronary angiograms showed a calcified lesion with 85% stenosis in the ostial LCx.

This patient's polar map (Fig. 5) revealed a large area of dark blue distributed through the basal-to-mid segments of the posterolateral wall that correlated with the LCx stenosis seen on the angiograms. This alerted the clinician to a degree of dysfunction and myocardium
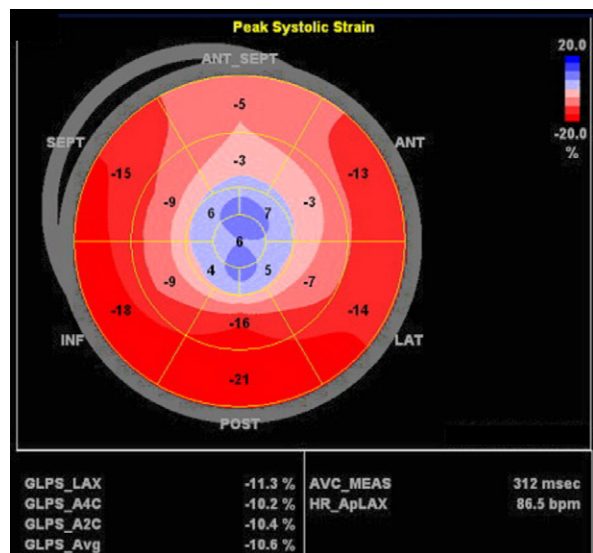
Fig. 3 *Patient 3. A polar map derived by speckle-tracking echocardiography shows the peak strain of longitudinal myocardial fibers in a patient with single-vessel disease of the left anterior descending coronary artery. The defect is seen in the progression from red and pink in the basal segments to blue in the apical segments.*

ANT = anterior; ANT_SEPT = anteroseptal; ApLAX = apical long axis; AVC = aortic valve closure; Avg = average; A2C = apical 2-chamber view; A4C = apical 4-chamber view; bpm = beats per minute; GLPS = global longitudinal peak strain; HR = heart rate; INF = inferior; LAT = lateral; LAX = long axis; MEAS = measurement; POST = posterior; SEPT = septal

Fig. 4 *Patient 4. A polar map derived by speckle-tracking echocardiography shows the peak systolic strain of longitudinal myocardial fibers in a patient with single-vessel disease of the right coronary artery. Note the progression from pink to light red in the basal-to-mid segments of the right coronary artery territory.*
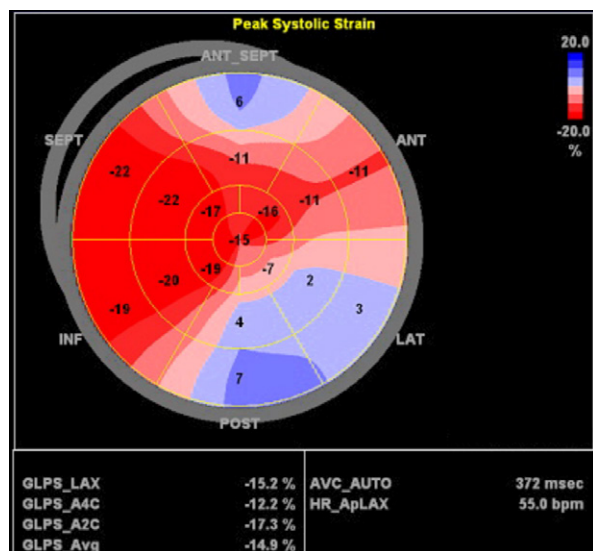
ANT = anterior; ANT_SEPT = anteroseptal; ApLAX = apical long axis; AVC = aortic valve closure; Avg = average; A2C = apical 2-chamber view; A4C = apical 4-chamber view; bpm = beats per minute; GLPS = global longitudinal peak strain; HR = heart rate; INF = inferior; LAT = lateral; LAX = long axis; MEAS = measurement; POST = posterior; SEPT = septal

at risk disproportionate to the relative mild dysfunction evidenced by the wall motion and LVEF alone.

Patient 6

Pseudo Left Circumflex Coronary Artery Disease. An 80-year-old woman presented with tachycardia and fatigue that had persisted for several weeks. Her medical history included left upper lobe adenocarcinoma treated by left upper lobectomy 11 years previously, CAD treated by PCI with 2 stents, and osteoporosis. A computed tomogram of the thorax revealed widespread metastatic disease in the supraclavicular, mediastinal, right mammary, and left hilar regions, and an apparent pericardial mass at the base of the lateral wall involving the pericardium and myocardium. An ECG showed sinus tachycardia with poor R-wave progression. An echocardiogram showed an LVEF of 0.60 to 0.65 and diffuse pericardial thickening.

This patient's polar map (Fig. 6A) revealed an abnormal pattern of LV peak systolic longitudinal strain at the location of infiltrative metastatic disease. The dark blue-to-pink pattern seen in the lateral and posterior wall segments of the map correlated with direct tumor infiltration of the myocardium, not with LCx stenosis as originally suspected. A chest computed tomogram (Fig. 6B) showed direct tumor infiltration of the myo-

cardium at the basal lateral wall, correlating with the territory affected by the defect shown on the polar map.

Patient 7

Leukemic Infiltration Imitating Amyloidosis. A 13-year-old boy with acute lymphocytic leukemia (ALL) presented with back pain and was admitted with bacteremia. His medical history included double-cord stem cell transplantation 6 months previously, complicated

Fig. 6 Patient 6. **A**) A polar map derived by speckle-tracking echocardiography shows the peak systolic strain of longitudinal myocardial fibers in a patient with pseudo left circumflex coronary artery disease. The distribution of blue in the lateral and posterior wall segments correlates with an area of tumor infiltration of the myocardium. **B**) A chest computed tomogram shows a mass (arrow) infiltrating the left ventricular basal lateral segments.

ANT = anterior; ANT_SEPT = anteroseptal; ApLAX = apical long axis; AVC = aortic valve closure; Avg = average; A2C = apical 2-chamber view; A4C = apical 4-chamber view; bpm = beats per minute; GLPS = global longitudinal peak strain; HR = heart rate; INF = inferior; LAT = lateral; LAX = long axis; MEAS = measurement; POST = posterior; SEPT = septal
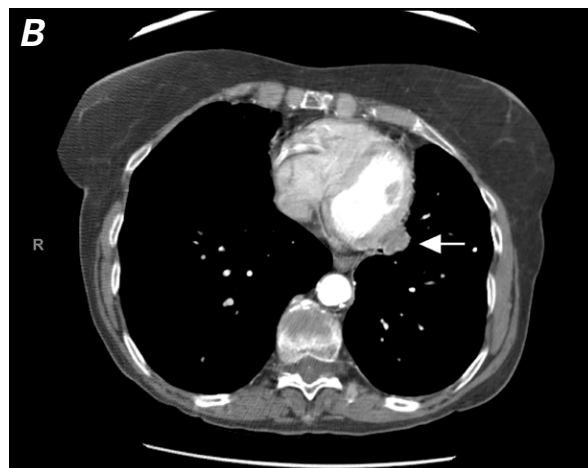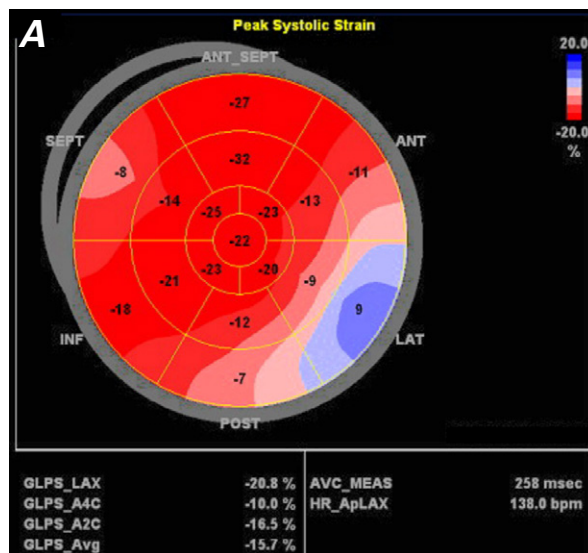
Fig. 5 Patient 5. A polar map derived by speckle-tracking echocardiography shows the peak systolic strain of longitudinal myocardial fibers in a patient with single-vessel disease of the left circumflex coronary artery. The distribution of blue in the lateral and posterior wall segments correlates with a defect in the circumflex coronary artery blood flow distribution.

ANT = anterior; ANT_SEPT = anteroseptal; ApLAX = apical long axis; Avg = average; AVC = aortic valve closure; AUTO = automated measurement; A2C = apical 2-chamber view; A4C = apical 4-chamber view; bpm = beats per minute; GLPS = global longitudinal peak strain; HR = heart rate; INF = inferior; LAT = lateral; LAX = long axis; POST = posterior; SEPT = septal

by multiple infections, gastrointestinal graft-versus-host disease, malnutrition, and weight loss. The patient's condition deteriorated after admission, and he experienced respiratory distress. A chest radiograph showed cardiomegaly. An echocardiogram was obtained and, on STE analysis, revealed the strain pattern shown in Figure 7. Subsequently, the patient was found to have leukemic infiltration of the heart, which led to complete atrioventricular block necessitating implantation of a permanent pacemaker and heart failure management.

The typical polar map in patients with amyloidosis shows dark red distributed in the apical segments and light red-to-blue in the surrounding segments, indicative of apical sparing. In this case, that pattern represented ALL infiltrating the myocardium and mimicking the strain pattern of amyloidosis (Fig. 7). Therefore, we think apical preservation can be a pattern of nonspecific infiltration, not specific to amyloidosis.

Patient 8

Chemotherapy-Related Cardiotoxicity. A 59-year-old woman with a history of hypertension, breast cancer (treated with pertuzumab, trastuzumab, and docetaxel, completed 6 months previously), and syncope due to dehydration had been monitored for cardiotoxicity while receiving trastuzumab. A baseline echocardiogram

Fig. 7 *Patient 7. A polar map derived by speckle-tracking echocardiography shows the peak systolic strain of longitudinal myocardial fibers in a patient with leukemic infiltration imitating amyloidosis. The distribution of dark red in the apical segments and light red-to-blue in the surrounding segments, a pattern indicative of apical sparing seen in amyloidosis, here indicates acute lymphocytic leukemia infiltrating the myocardium.*

ANT = anterior; ANT_SEPT = anteroseptal; ApLAX = apical long axis; Avg = average; AVC = aortic valve closure; AUTO = automated measurement; A2C = apical 2-chamber view; A4C = apical 4-chamber view; bpm = beats per minute; FR = frame rate; fps = frames per second; GLPS = global longitudinal peak strain; HR = heart rate; INF = inferior; LAT = lateral; LAX = long axis; POST = posterior; SEPT = septal

showed an LVEF of 0.59 and, on STE analysis, a GLS of −19%. Three months later, the patient's LVEF was unchanged, but her GLS had decreased to −15.2% (Fig. 8). Then, 3 months after that, a follow-up echocardiogram showed an LVEF of 0.44.

The polar map at 3-month follow-up revealed somewhat patchy but almost global depression in strain percentages with normal LVEF. This first sign of myocardial dysfunction was seen 3 months before the dysfunction became evident by conventional LVEF measurement.

Patient 9

Stress-Induced Cardiomyopathy. A 77-year-old man with a history of pancreatic cancer metastatic to the liver, dyslipidemia, cerebrovascular accident, left-lower-extremity deep vein thrombosis, and gastrointestinal bleeding was admitted for fever and abdominal pain. Results of radiologic studies done on arrival showed biliary obstruction, leading to cholangitis and possible mesenteric ischemia with progression of the metastatic pancreatic cancer. An abdominal left external biliary drain was placed soon after admission, and sepsis secondary to ascending cholangitis was found. Cardiac enzyme levels were mildly elevated. An ECG showed sinus rhythm, moderate intraventricular conduction delay, ST-segment deviation, and moderate T-wave abnormality in the anterolateral leads. An echocardiogram

Fig. 8 *Patient 8. A polar map derived by speckle-tracking echocardiography shows the peak systolic strain of longitudinal myocardial fibers in a patient with chemotherapy-related cardiotoxicity. Note the patchy, almost global depression in strain percentages.*
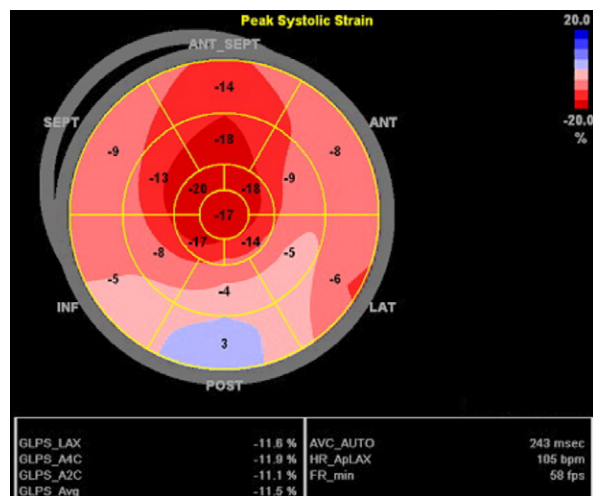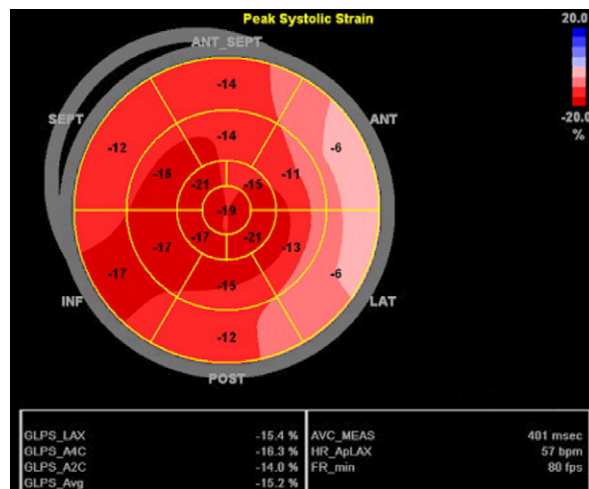
ANT = anterior; ANT_SEPT = anteroseptal; ApLAX = apical long axis; AVC = aortic valve closure; Avg = average; A2C = apical 2-chamber view; A4C = apical 4-chamber view; bpm = beats per minute; FR = frame rate; fps = frames per second; GLPS = global longitudinal peak strain; HR = heart rate; INF = inferior; LAT = lateral; LAX = long axis; MEAS = measurement; POST = posterior; SEPT = septal

revealed an LVEF of 0.40 to 0.45 and a wall-motion pattern consistent with stress-induced (takotsubo) cardiomyopathy, or apical ballooning syndrome.

In this case, the polar map pattern was the reverse of that seen for apical preservation in classic amyloidosis (Fig. 9). The blue-to-pink distribution in the mid-to-apical segments correlated with the apical ballooning. The dark red in the basal segments correlated with preserved basal myocardial function.

Patient 10

Suspected Infiltrative Process, Increased Left Ventricular Mass. A 52-year-old woman presented for evaluation of abnormal echocardiographic findings. Her medical history included hypertension, low-grade B-cell lymphoma with plasmacytic differentiation treated by autologous stem cell transplantation, amyloid deposition, rheumatoid arthritis, Sjögren disease, thymoma treated by resection, and Waldenström macroglobulinemia. A progressive increase in LV mass had been noted on echocardiograms over the previous 7 months. The most recent echocardiogram appeared to show an infiltrative or increased mass of the LV.

The patient's polar map revealed an intense red pattern with the highest deformation values in the apical segments, indicating apical preservation (Fig. 10). An endomyocardial biopsy was negative for amyloid on 2 separate occasions 2 years apart.
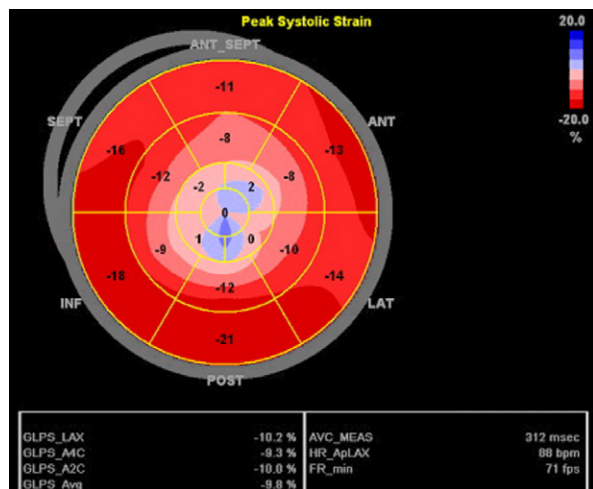
Patient 11

Amyloidosis. A 53-year-old man with a medical history of hypertension, dyslipidemia, atrial fibrillation, multiple myeloma treated by autologous stem cell transplantation, and cardiac amyloidosis presented with lower-extremity edema. He reported no chest pain, shortness of breath, paroxysmal nocturnal dyspnea, or orthopnea. An ECG showed low voltage. An echocardiogram showed an LVEF of 0.40 and, on STE analysis, a strain pattern indicative of amyloidosis. Of note, previous left-sided heart catheterization had revealed normal coronary arteries.

This patient's polar map revealed the classic bull's-eye pattern seen in cardiac amyloidosis (Fig. 11). The dark red at the apex and the surrounding pink-to-blue distribution indicated apical preservation.

Conclusion

Incorporating strain analysis into echocardiography has provided substantial diagnostic and prognostic benefit to the field of cardio-oncology. Myocardial deformation assessment by STE, an angle-independent method,
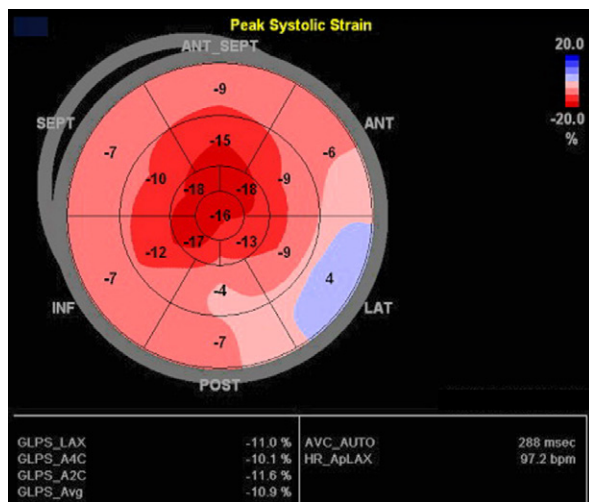

Fig. 9 *Patient 9. A polar map derived by speckle-tracking echocardiography shows the peak systolic strain of longitudinal myocardial fibers in a patient with stress-induced cardiomyopathy. This is evidenced by the distribution of blue from the mid to apical region. The dark red in the basal segments correlates with preserved basal myocardial function.*

ANT = anterior; ANT_SEPT = anteroseptal; ApLAX = apical long axis; AVC = aortic valve closure; Avg = average; A2C = apical 2-chamber view; A4C = apical 4-chamber view; bpm = beats per minute; FR = frame rate; fps = frames per second; GLPS = global longitudinal peak strain; HR = heart rate; INF = inferior; LAT = lateral; LAX = long axis; MEAS = measurement; POST = posterior; SEPT = septal
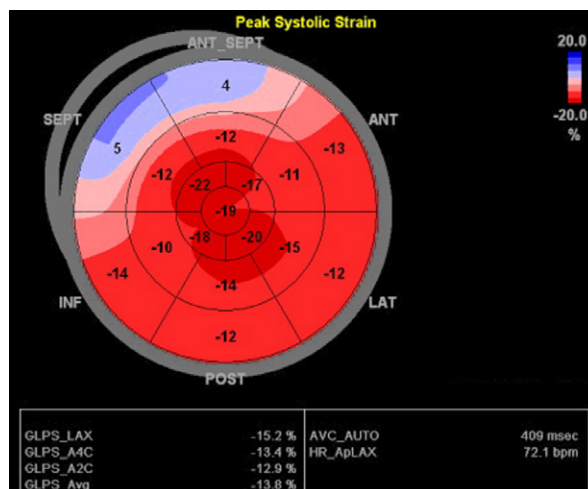
Fig. 10 *Patient 10. A polar map derived by speckle-tracking echocardiography shows the peak systolic strain of longitudinal myocardial fibers in a patient with a suspected infiltrative process and increased left ventricular mass. Apical preservation is evidenced by the intense red area with the highest deformation values in the apical segments.*

ANT = anterior; ANT_SEPT = anteroseptal; ApLAX = apical long axis; Avg = average; AVC = aortic valve closure; AUTO = automated measurement; A2C = apical 2-chamber view; A4C = apical 4-chamber view; bpm = beats per minute; GLPS = global longitudinal peak strain; HR = heart rate; INF = inferior; LAT = lateral; LAX = long axis; POST = posterior; SEPT = septal

Fig. 11 *Patient 11. A polar map derived by speckle-tracking echocardiography shows the peak systolic strain of longitudinal myocardial fibers in a patient with amyloidosis. This classic pattern with apical preservation is indicated by the dark red pattern in the apical segment and the surrounding pink-to-blue color distribution.*

ANT = anterior; ANT_SEPT = anteroseptal; ApLAX = apical long axis; Avg = average; AVC = aortic valve closure; AUTO = automated measurement; A2C = apical 2-chamber view; A4C = apical 4-chamber view; bpm = beats per minute; GLPS = global longitudinal peak strain; HR = heart rate; INF = inferior; LAT = lateral; LAX = long axis; POST = posterior; SEPT = septal

can enable detection of subclinical LV dysfunction before it is perceptible by conventional echocardiography. Because STE is nontoxic and entails no exposure to ionizing radiation, it should be considered the cardiac imaging method of choice in most centers. However, it has certain limitations. Speckle tracking–derived strain is profoundly dependent on image quality throughout the cardiac cycle. In addition, the different strain patterns described in the case reports presented here are not entirely specific for any given cardiovascular condition. Thus, STE cannot be used to establish a cause of disease without clinical correlation. Further research to better understand the full potential of myocardial strain imaging by STE and its interpretation in cardio-oncologic care is warranted.

Acknowledgments

References

1. Ballester-Rodés M, Flotats A, Torrent-Guasp F, Carrió-Gasset I, Ballester-Alomar M, Carreras F, et al. The sequence of regional ventricular motion. Eur J Cardiothorac Surg 2006;29 Suppl 1:S139-44.
2. Dandel M, Lehmkuhl H, Knosalla C, Suramelashvili N, Hetzer R. Strain and strain rate imaging by echocardiography - basic concepts and clinical applicability. Curr Cardiol Rev 2009;5(2):133-48.
3. Hoit BD. Strain and strain rate echocardiography and coronary artery disease. Circ Cardiovasc Imaging 2011;4(2):179-90.
4. Urheim S, Edvardsen T, Torp H, Angelsen B, Smiseth OA. Myocardial strain by Doppler echocardiography. Validation of a new method to quantify regional myocardial function. Circulation 2000;102(10):1158-64.
5. Villarraga HR, Herrmann J, Nkomo VT. Cardio-oncology: role of echocardiography. Prog Cardiovasc Dis 2014;57(1):10-8.
6. Ingul CB, Torp H, Aase SA, Berg S, Stoylen A, Slordahl SA. Automated analysis of strain rate and strain: feasibility and clinical implications. J Am Soc Echocardiogr 2005;18(5):411-8.
7. Yingchoncharoen T, Agarwal S, Popovic ZB, Marwick TH. Normal ranges of left ventricular strain: a meta-analysis. J Am Soc Echocardiogr 2013;26(2):185-91.
8. Bansal M, Cho GY, Chan J, Leano R, Haluska BA, Marwick TH. Feasibility and accuracy of different techniques of two-dimensional speckle based strain and validation with harmonic phase magnetic resonance imaging. J Am Soc Echocardiogr 2008;21(12):1318-25.
9. Kalam K, Otahal P, Marwick TH. Prognostic implications of global LV dysfunction: a systematic review and meta-analysis of global longitudinal strain and ejection fraction. Heart 2014;100(21):1673-80.
10. Siegel RL, Miller KD, Jemal A. Cancer statistics, 2017. CA Cancer J Clin 2017;67(1):7-30.
11. Poterucha JT, Kutty S, Lindquist RK, Li L, Eidem BW. Changes in left ventricular longitudinal strain with anthracycline chemotherapy in adolescents precede subsequent decreased left ventricular ejection fraction. J Am Soc Echocardiogr 2012;25(7):733-40.
12. Negishi K, Negishi T, Hare JL, Haluska BA, Plana JC, Marwick TH. Independent and incremental value of deformation indices for prediction of trastuzumab-induced cardiotoxicity. J Am Soc Echocardiogr 2013;26(5):493-8.
13. Mornos C, Petrescu L. Early detection of anthracycline-mediated cardiotoxicity: the value of considering both global longitudinal left ventricular strain and twist. Can J Physiol Pharmacol 2013;91(8):601-7.
14. Toro-Salazar OH, Ferranti J, Lorenzoni R, Walling S, Mazur W, Raman SV, et al. Feasibility of echocardiographic techniques to detect subclinical cancer therapeutics-related cardiac dysfunction among high-dose patients when compared with cardiac magnetic resonance imaging. J Am Soc Echocardiogr 2016;29(2):119-31.
15. Plana JC, Galderisi M, Barac A, Ewer MS, Ky B, Scherrer-Crosbie M, et al. Expert consensus for multimodality imaging evaluation of adult patients during and after cancer therapy: a report from the American Society of Echocardiography and the European Association of Cardiovascular Imaging. J Am Soc Echocardiogr 2014;27(9):911-39.
16. Fallah-Rad N, Walker JR, Wassef A, Lytwyn M, Bohonis S, Fang T, et al. The utility of cardiac biomarkers, tissue velocity and strain imaging, and cardiac magnetic resonance imaging in predicting early left ventricular dysfunction in patients with human epidermal growth factor receptor II-positive breast cancer treated with adjuvant trastuzumab therapy. J Am Coll Cardiol 2011;57(22):2263-70.
17. Sawaya H, Sebag IA, Plana JC, Januzzi JL, Ky B, Cohen V, et al. Early detection and prediction of cardiotoxicity in chemotherapy-treated patients. Am J Cardiol 2011;107(9):1375-80.

18. Thavendiranathan P, Poulin F, Lim KD, Plana JC, Woo A, Marwick TH. Use of myocardial strain imaging by echocardiography for the early detection of cardiotoxicity in patients during and after cancer chemotherapy: a systematic review. J Am Coll Cardiol 2014;63(25 Pt A):2751-68.

19. Negishi K, Negishi T, Haluska BA, Hare JL, Plana JC, Marwick TH. Use of speckle strain to assess left ventricular responses to cardiotoxic chemotherapy and cardioprotection. Eur Heart J Cardiovasc Imaging 2014;15(3):324-31.

20. Yusuf SW, Howell RM, Gomez D, Pinnix CC, Iliescu CA, Banchs J. Radiation-related heart and vascular disease. Future Oncol 2015;11(14):2067-76.

21. Darby SC, Ewertz M, McGale P, Bennet AM, Blom-Goldman U, Bronnum D, et al. Risk of ischemic heart disease in women after radiotherapy for breast cancer. N Engl J Med 2013;368(11):987-98.

22. Taunk NK, Haffty BG, Kostis JB, Goyal S. Radiation-induced heart disease: pathologic abnormalities and putative mechanisms. Front Oncol 2015;5:39.

23. Orzan F, Brusca A, Conte MR, Presbitero P, Figliomeni MC. Severe coronary artery disease after radiation therapy of the chest and mediastinum: clinical presentation and treatment. Br Heart J 1993;69(6):496-500.

24. Hull MC, Morris CG, Pepine CJ, Mendenhall NP. Valvular dysfunction and carotid, subclavian, and coronary artery disease in survivors of Hodgkin lymphoma treated with radiation therapy. JAMA 2003;290(21):2831-7.

25. Correa CR, Litt HI, Hwang WT, Ferrari VA, Solin LJ, Harris EE. Coronary artery findings after left-sided compared with right-sided radiation treatment for early-stage breast cancer. J Clin Oncol 2007;25(21):3031-7.

26. Favourable and unfavourable effects on long-term survival of radiotherapy for early breast cancer: an overview of the randomised trials. Early Breast Cancer Trialists' Collaborative Group. Lancet 2000;355(9217):1757-70.

27. Biering-Sorensen T, Hoffmann S, Mogelvang R, Zeeberg Iversen A, Galatius S, Fritz-Hansen T, et al. Myocardial strain analysis by 2-dimensional speckle tracking echocardiography improves diagnostics of coronary artery stenosis in stable angina pectoris. Circ Cardiovasc Imaging 2014;7(1):58-65.

28. Lo Q, Hee L, Batumalai V, Allman C, MacDonald P, Delaney GP, et al. Subclinical cardiac dysfunction detected by strain imaging during breast irradiation with persistent changes 6 weeks after treatment. Int J Radiat Oncol Biol Phys 2015;92(2):268-76.

29. Lo Q, Hee L, Batumalai V, Allman C, MacDonald P, Lonergan D, et al. Strain imaging detects dose-dependent segmental cardiac dysfunction in the acute phase after breast irradiation. Int J Radiat Oncol Biol Phys 2017;99(1):182-90.

30. Gagliardi G, Constine LS, Moiseenko V, Correa C, Pierce LJ, Allen AM, Marks LB. Radiation dose-volume effects in the heart. Int J Radiat Oncol Biol Phys 2010;76(3 Suppl):S77-85.

31. Tsai HR, Gjesdal O, Wethal T, Haugaa KH, Fossa A, Fossa SD, Edvardsen T. Left ventricular function assessed by two-dimensional speckle tracking echocardiography in long-term survivors of Hodgkin's lymphoma treated by mediastinal radiotherapy with or without anthracycline therapy. Am J Cardiol 2011;107(3):472-7.

32. Nolan MT, Russell DJ, Marwick TH. Long-term risk of heart failure and myocardial dysfunction after thoracic radiotherapy: a systematic review. Can J Cardiol 2016;32(7):908-20.

33. Jacob S, Pathak A, Franck D, Latorzeff I, Jimenez G, Fondard O, et al. Early detection and prediction of cardiotoxicity after radiation therapy for breast cancer:

the BACCARAT prospective cohort study. Radiat Oncol 2016;11:54.

34. Kyle RA, Greipp PR. Amyloidosis (AL). Clinical and laboratory features in 229 cases. Mayo Clin Proc 1983;58(10):665-83.

35. Kyle RA, Greipp PR, O'Fallon WM. Primary systemic amyloidosis: multivariate analysis for prognostic factors in 168 cases. Blood 1986;68(1):220-4.

36. Merlini G, Bellotti V. Molecular mechanisms of amyloidosis. N Engl J Med 2003;349(6):583-96.

37. Yusuf SW, Negi SI, Lenihan DJ. Infiltrative cardiomyopathy and pericardial disease. Semin Oncol 2013;40(2):199-209.

38. Esposito BP, Breuer W, Sirankapracha P, Pootrakul P, Hershko C, Cabantchik ZI. Labile plasma iron in iron overload: redox activity and susceptibility to chelation. Blood 2003;102(7):2670-7.

39. Petersen CD, Robinson WA, Kurnick JE. Involvement of the heart and pericardium in the malignant lymphomas. Am J Med Sci 1976;272(2):161-5.

40. Anderson LJ, Holden S, Davis B, Prescott E, Charrier CC, Bunce NH, et al. Cardiovascular T2-star (T2*) magnetic resonance for the early diagnosis of myocardial iron overload. Eur Heart J 2001;22(23):2171-9.

41. Aessopos A, Fragodimitri C, Karabatsos F, Hatziliami A, Yousef J, Giakoumis A, et al. Cardiac magnetic resonance imaging R2* assessments and analysis of historical parameters in patients with transfusion-dependent thalassemia. Haematologica 2007;92(1):131-2.

42. Di Odoardo LAF, Giuditta M, Cassinerio E, Roghi A, Pedrotti P, Vicenzi M, et al. Myocardial deformation in iron overload cardiomyopathy: speckle tracking imaging in a beta-thalassemia major population. Intern Emerg Med 2017;12(6):799-809.

43. Chen MR, Ko HS, Chao TF, Liu HC, Kuo JY, Bulwer BE, et al. Relation of myocardial systolic mechanics to serum ferritin level as a prognosticator in thalassemia patients undergoing repeated transfusion. Echocardiography 2015;32(1):79-88.

44. Phelan D, Collier P, Thavendiranathan P, Popovic ZB, Hanna M, Plana JC, et al. Relative apical sparing of longitudinal strain using two-dimensional speckle-tracking echocardiography is both sensitive and specific for the diagnosis of cardiac amyloidosis. Heart 2012;98(19):1442-8.

45. Quintana-Quezada RA, Yusuf SW, Banchs J. Use of noninvasive imaging in cardiac amyloidosis. Curr Treat Options Cardiovasc Med 2016;18(7):46.

46. Buss SJ, Emami M, Mereles D, Korosoglou G, Kristen AV, Voss A, et al. Longitudinal left ventricular function for prediction of survival in systemic light-chain amyloidosis: incremental value compared with clinical and biochemical markers. J Am Coll Cardiol 2012;60(12):1067-76.

47. Ternacle J, Bodez D, Guellich A, Audureau E, Rappeneau S, Lim P, et al. Causes and consequences of longitudinal LV dysfunction assessed by 2D strain echocardiography in cardiac amyloidosis. JACC Cardiovasc Imaging 2016;9(2):126-38.

48. Fajardo LF, Stewart JR, Cohn KE. Morphology of radiation-induced heart disease. Arch Pathol 1968;86(5):512-9.

49. Adams MJ, Lipsitz SR, Colan SD, Tarbell NJ, Treves ST, Diller L, et al. Cardiovascular status in long-term survivors of Hodgkin's disease treated with chest radiotherapy. J Clin Oncol 2004;22(15):3139-48.

50. Heidenreich PA, Hancock SL, Lee BK, Mariscal CS, Schnittger I. Asymptomatic cardiac disease following mediastinal irradiation. J Am Coll Cardiol 2003;42(4):743-9.

51. Cella L, Liuzzi R, Conson M, Torre G, Caterino M, De Rosa N, et al. Dosimetric predictors of asymptomatic heart

valvular dysfunction following mediastinal irradiation for Hodgkin's lymphoma. Radiother Oncol 2011;101(2):316-21.

52. Machann W, Beer M, Breunig M, Stork S, Angermann C, Seufert I, et al. Cardiac magnetic resonance imaging findings in 20-year survivors of mediastinal radiotherapy for Hodgkin's disease. Int J Radiat Oncol Biol Phys 2011;79(4):1117-23.

53. Cutter DJ, Schaapveld M, Darby SC, Hauptmann M, van Nimwegen FA, Krol AD, et al. Risk of valvular heart disease after treatment for Hodgkin lymphoma. J Natl Cancer Inst 2015;107(4).

54. Aleman BM, van den Belt-Dusebout AW, De Bruin ML, van 't Veer MB, Baaijens MH, de Boer JP, et al. Late cardiotoxicity after treatment for Hodgkin lymphoma. Blood 2007;109(5):1878-86.

55. van Nimwegen FA, Schaapveld M, Janus CP, Krol AD, Petersen EJ, Raemaekers JM, et al. Cardiovascular disease after Hodgkin lymphoma treatment: 40-year disease risk. JAMA Intern Med 2015;175(6):1007-17.

56. Murbraech K, Wethal T, Smeland KB, Holte H, Loge JH, Holte E, et al. Valvular dysfunction in lymphoma survivors treated with autologous stem cell transplantation: a national cross-sectional study. JACC Cardiovasc Imaging 2016;9(3):230-9.

57. Nishimura RA, Otto CM, Bonow RO, Carabello BA, Erwin JP 3rd, Guyton RA, et al. 2014 AHA/ACC guideline for the management of patients with valvular heart disease: a report of the American College of Cardiology/American Heart Association Task Force on Practice Guidelines [published erratum appears in J Am Coll Cardiol 2014;63(22):2489]. J Am Coll Cardiol 2014;63(22):e57-185.

58. Nishimura RA, Otto CM, Bonow RO, Carabello BA, Erwin JP 3rd, Fleisher LA, et al. 2017 AHA/ACC focused update of the 2014 AHA/ACC guideline for the management of patients with valvular heart disease: a report of the American College of Cardiology/American Heart Association Task Force on Clinical Practice Guidelines. J Am Coll Cardiol 2017;70(2):252-89.

59. Witkowski TG, Thomas JD, Debonnaire PJ, Delgado V, Hoke U, Ewe SH, et al. Global longitudinal strain predicts left ventricular dysfunction after mitral valve repair. Eur Heart J Cardiovasc Imaging 2013;14(1):69-76.

60. Witkowski TG, Thomas JD, Delgado V, van Rijnsoever E, Ng AC, Hoke U, et al. Changes in left ventricular function after mitral valve repair for severe organic mitral regurgitation. Ann Thorac Surg 2012;93(3):754-60.

61. Magne J, Mahjoub H, Dulgheru R, Pibarot P, Pierard LA, Lancellotti P. Left ventricular contractile reserve in asymptomatic primary mitral regurgitation. Eur Heart J 2014;35(24):1608-16.

62. Alashi A, Mentias A, Abdallah A, Feng K, Gillinov AM, Rodriguez LL, et al. Incremental prognostic utility of left ventricular global longitudinal strain in asymptomatic patients with significant chronic aortic regurgitation and preserved left ventricular ejection fraction. JACC Cardiovasc Imaging 2018;11(5):673-82.

63. Yingchoncharoen T, Gibby C, Rodriguez LL, Grimm RA, Marwick TH. Association of myocardial deformation with outcome in asymptomatic aortic stenosis with normal ejection fraction. Circ Cardiovasc Imaging 2012;5(6):719-25.

64. Kusunose K, Goodman A, Parikh R, Barr T, Agarwal S, Popovic ZB, et al. Incremental prognostic value of left ventricular global longitudinal strain in patients with aortic stenosis and preserved ejection fraction. Circ Cardiovasc Imaging 2014;7(6):938-45.

65. Sogaard KK, Farkas DK, Ehrenstein V, Bhaskaran K, Botker HE, Sorensen HT. Pericarditis as a marker of occult cancer and a prognostic factor for cancer mortality. Circulation 2017;136(11):996-1006.

66. Veinot JP, Edwards WD. Pathology of radiation-induced heart disease: a surgical and autopsy study of 27 cases. Hum Pathol 1996;27(8):766-73.

67. Chello M, Mastroroberto P, Romano R, Zofrea S, Bevacqua I, Marchese AR. Changes in the proportion of types I and III collagen in the left ventricular wall of patients with post-irradiative pericarditis. Cardiovasc Surg 1996;4(2):222-6.

68. Beukema JC, van Luijk P, Widder J, Langendijk JA, Muijs CT. Is cardiac toxicity a relevant issue in the radiation treatment of esophageal cancer? Radiother Oncol 2015;114(1):85-90.

69. Ling LH, Oh JK, Schaff HV, Danielson GK, Mahoney DW, Seward JB, Tajik AJ. Constrictive pericarditis in the modern era: evolving clinical spectrum and impact on outcome after pericardiectomy. Circulation 1999;100(13):1380-6.

70. Sengupta PP, Krishnamoorthy VK, Abhayaratna WP, Korinek J, Belohlavek M, Sundt TM 3rd, et al. Disparate patterns of left ventricular mechanics differentiate constrictive pericarditis from restrictive cardiomyopathy. JACC Cardiovasc Imaging 2008;1(1):29-38.

71. Bottinor WJ, Migliore CK, Lenneman CA, Stoddard MF. Echocardiographic assessment of cardiotoxic effects of cancer therapy. Curr Cardiol Rep 2016;18(10):99.

72. Leitman M, Bachner-Hinenzon N, Adam D, Fuchs T, Theodorovich N, Peleg E, et al. Speckle tracking imaging in acute inflammatory pericardial diseases. Echocardiography 2011;28(5):548-55.